Supporting Information

Hu et al. 10.1073/pnas.1503861112

S1. LPCS Setup and Process

An *xyz* piezoelectric nanotranslation stage (P545; Physik Instrumente) is used to trace out the pillar structures in the photoresist while the laser focus remains immobile. The objective, nanotranslation stage, and CCD camera for in situ observation are mounted in a modified optical microscope (BX51; Olympus). A mechanical shutter (SH05; Thorlabs) is used to control the beam during the material processing and the combination of a waveplate and a polarizer is used to attenuate the laser power. In the main text, an average power of 85 mW is applied for the pillar structures fabrication unless stated otherwise (measured before microscope, and it should be noted that the optics and objective in the microscope will cause a certain power loss). The detailed process is shown in Fig. S1. Photoresist is first drop-cast onto a cover glass and then baked on a hotplate at 100 °C for 1 h to remove solvents and form a gel. A femtosecond laser beam is used to irradiate the sample to fabricate the pillar array. After polymerization, the sample is developed in 1-propanol for 20 min. Then the sample is pulled out and the developer evaporates, during which the pillars assemble into ordered hierarchical structures with the aid of capillary force. Note that the total area of structures is determined merely by the translation stage; a long-range stage can be chosen to ensure the submicron pillars assemble into microscale cells over several centimeters and then large-area hierarchical structures can be generated by LPCS. Parallel laser printing techniques (1, 2) can also be used to ensure rapid fabrication across such a large area.

S2. Sample Characterization

The morphologies of the assembled microarchitectures are characterized by a field emission scanning electron microscope (Sirion 200; FEI). Before imaging, the samples are sputtered with a thin layer of gold. The fluorescent images of the structures are taken by an inverted microscope with fluorescence (DMI 3000B; Leica), where an excitation filter of 450–490 nm is used. The videos of the micropillar array self-organization and recovery are recorded by the Leica microscope in bright-field mode. The other optical characterizations of the samples and the in situ observations of microparticle trapping and releasing are performed on an Olympus BX51microscope.

S3. Quantitative Discussion on the Capillary Force, Elastic Restoring Force, Bond Number, and Effect of Gravity

In the main text we only discuss the forces in two critical cases (before the pillars bend and after their tips contact). Here we perform a quantitative study on the various forces during the pillar assembling process. The capillary force is given by $F_C = 2\pi\gamma r^2 \cos^2\theta/u$, where u is the distance between two pillar tips and dynamically changes when the pillars are bending. For the liquid 1-propanol, the interfacial tension γ = 25.26 mN/m. The radius of pillars r = 380 nm can be measured from SEM images. The distance between two pillar tips in the initial state is $u = d$ = 3 μm. Thus, for a typical case of θ = 60°, the capillary force is 1.91 nN when the pillars stand upright. The distance u decreases sharply as the pillars bend (it reaches zero when the top ends of two pillars contact) and hence the capillary force increases rapidly. According to previous studies (3, 4), it is reasonable to estimate the capillary force increases by more than three orders of magnitude at the last moment before two pillars contact (van de Waals interactions begin to take effect in nanometer scale). Thus, the maximum capillary force is probably ∼2 μN. The elastic restoring force is given by $F_S = 3\pi E r^4 v/4h^3$, where v is the horizontal displacement of the pillar tip from its base. So, F_s = 0 when the pillar is upright at the beginning. For the photoresist SZ2080 used here, E = 1∼2 GPa (5). Therefore, the maximum elastic force F_s is 1.15∼2.3 μN (when $v = d/2$ = 1.5 μm and h = 4 μm), which is comparable to the magnitude of the maximum capillary force. Hence, slightly tuning the geometry or the distribution of the pillars may induce controllable self-assemblies. Bond number is a dimensionless number to show the importance of surface tension forces compared with body forces (e.g., gravity) (6). Here $Bo = \rho g(d/2)^2/\gamma = 6.98 \times 10^{-7}$. The extremely small value (<<1) of the Bond number indicates that surface tension dominates the system and the effect of gravity is negligible. Specifically, the gravity of an individual pillar is around 1.8×10^{-5} nN, resulting in a torque T_g ∼1.4×10^{-20} N·m on the pillars. The torque from the capillary force T_c ∼8×10^{-12} N·m, is larger than T_g by eight orders of magnitude. Therefore, the effect of gravity can be neglected in this scale.

S4. Influence of the Microparticle on the Capillary Force Acting on Micropillars

When the particles are put into the solvent with pillar arrays, a number of particles drift into the designed cells and a new pillar–particle–pillar system is built, as shown in Fig. S5. A meniscus connecting the pillar and particle is formed, resulting in an extra capillary force. Because the distance between pillar and particle is very small, the pillar–particle capillary force is extremely strong. From the SEM images in Fig. 5*B* we can observe a slight difference between the shape of assembled cells with a particle and the empty ones, caused by the relatively strong pillar–particle capillary force. More obvious difference can be observed in Fig. S5. This phenomenon actually further benefits the trapping efficiency because the new capillary force inside the cell makes it much easier to trap the particle.

1. Hu Y, et al. (2013) High-efficiency fabrication of aspheric microlens arrays by holographic femtosecond laser-induced photopolymerization. *Appl Phys Lett* 103(14):141112.
2. Lin H, Jia B, Gu M (2011) Dynamic generation of Debye diffraction-limited multifocal arrays for direct laser printing nanofabrication. *Opt Lett* 36(3):406–408.
3. Chandra D, Yang S (2009) Capillary-force-induced clustering of micropillar arrays: Is it caused by isolated capillary bridges or by the lateral capillary meniscus interaction force? *Langmuir* 25(18):10430–10434.
4. Pokroy B, Kang SH, Mahadevan L, Aizenberg J (2009) Self-organization of a mesoscale bristle into ordered, hierarchical helical assemblies. *Science* 323(5911):237–240.
5. Skarmoutsou A, et al. (2013) Nanomechanical properties of hybrid coatings for bone tissue engineering. *J Mech Behav Biomed Mater* 25:48–62.
6. Hager WH (2012) Wilfrid Noel Bond and the Bond number. *J Hydraul Res* 50(1):3–9.

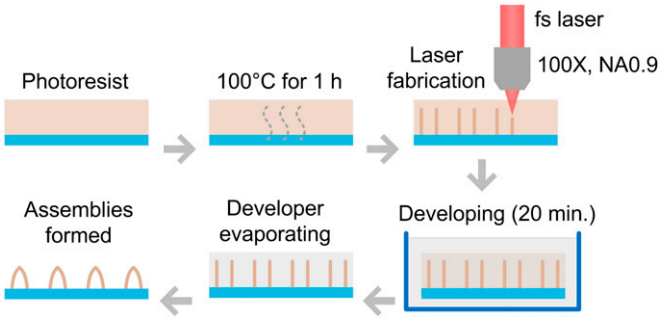

Fig. S1. Scheme of the LPCS fabrication process.

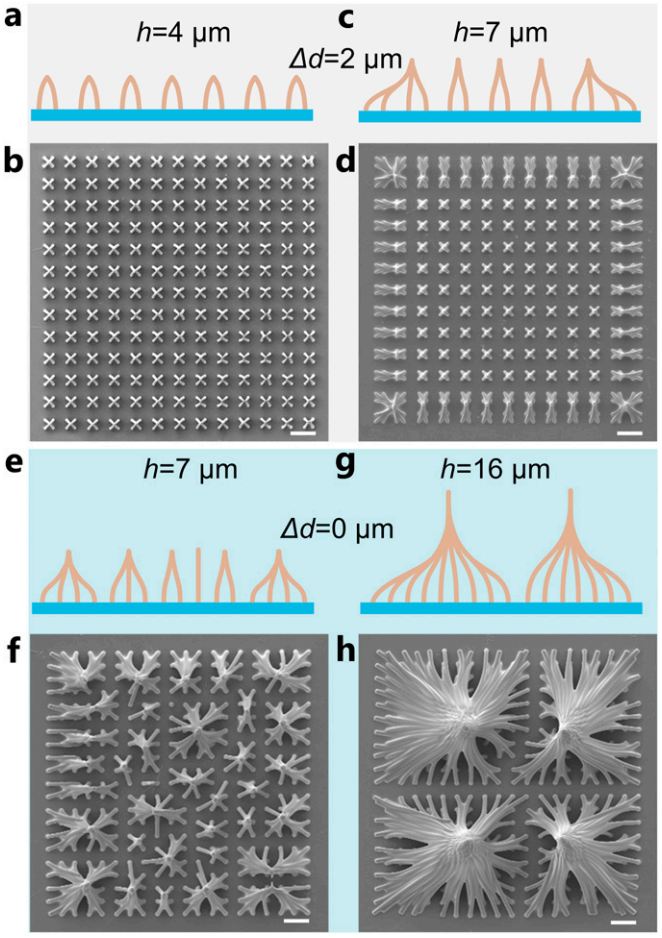

Fig. S2. Schematic diagrams and SEM images of different assemblies when the conditions change. (*A* and *B*) $h = 4$ μm and $\Delta d = 2$ μm. A uniform four-pillar assembly is formed. (*C* and *D*) $h = 7$ μm and $\Delta d = 2$ μm. Boundary pillars assemble into 8- or 16-pillar cells owing to the larger capillary force. As the liquid dries, the evaporation front first reaches the boundary and forms a liquid drop around the array. The boundary pillars receive an asymmetric capillary force from the neighboring pillars and the substrates. The capillary force between the pillar and the substrate is much smaller than those between pillars and therefore the total force on boundary pillars is larger than central ones. (*E* and *F*) $h = 7$ μm and $\Delta d = 0$. Boundary pillars assemble into relatively larger unit cells than the central pillars and the assembly is random owing to the equal distance between pillars. (*G* and *H*) $h = 16$ μm and $\Delta d = 0$. Large filamentous aggregates with four nucleated centers are generated. (Scale bars, 10 μm.)

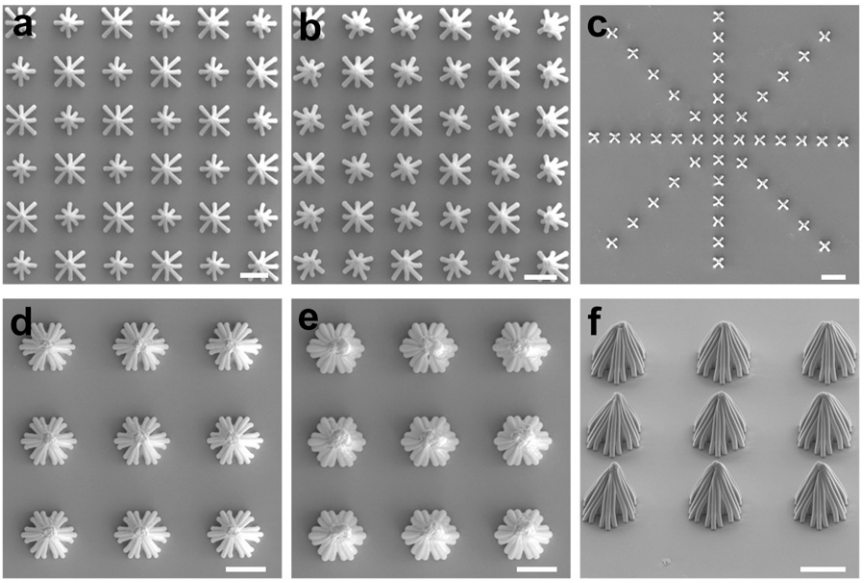

Fig. S3. Other examples of LPCS-prepared highly ordered self-assemblies. (*A*) Nine-pillar cells with different sizes and two rotation angles: 0° and 45°. (*B*) Nine-pillar cells with different sizes and three rotation angles: 0°, 30° and 60°. (Scale bars, 5 μm.) (*C*) Four-pillar cells are arranged in a pattern. (Scale bars, 10 μm.) (*D* and *E*) Daisy-like structures prepared using higher exposure power than those shown in Fig. 3: 95 and 115 mW, respectively. (*F*) Angled view of the daisy-like assemblies. (Scale bars, 10 μm.)

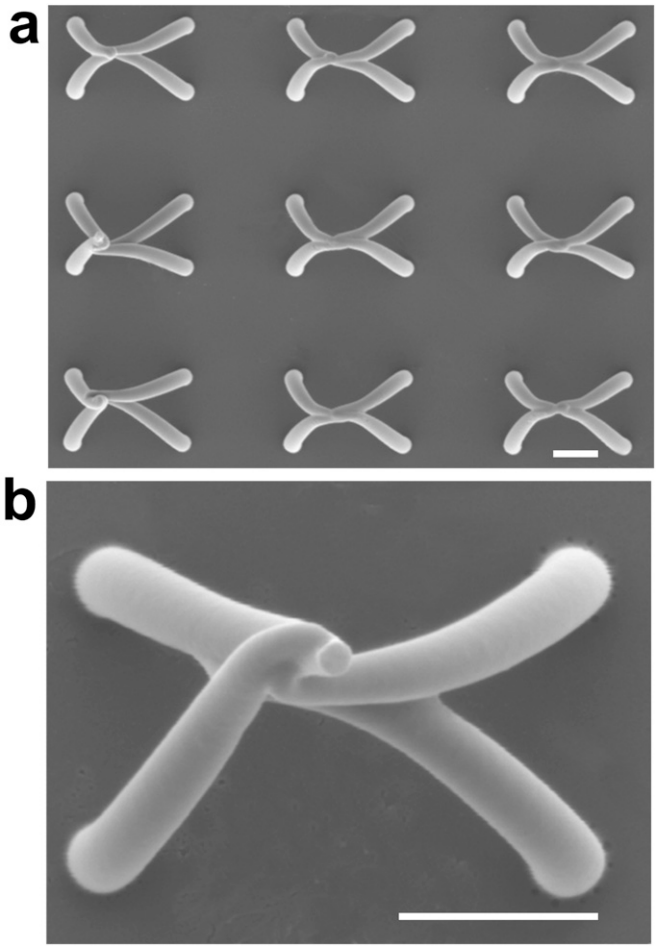

Fig. S4. SEM images showing the formation of helical patterns when increasing the pillar height. (*A*) The adjacent two-pillar cells further assemble into a four-pillar cell as the height of pillars is increased to 9 μm. (*B*) Magnified image showing the helical pattern beginning to appear. (Scale bars, 2 μm.)

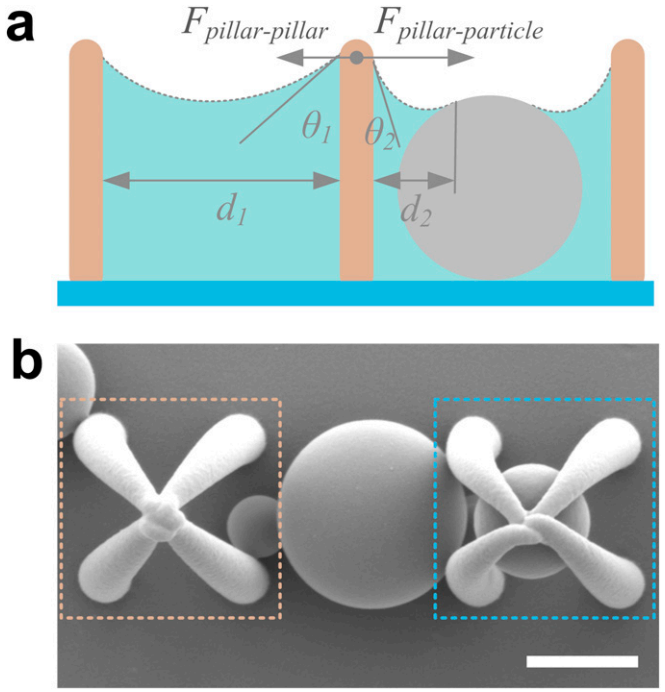

Fig. S5. (*A*) Schematic illustration of the geometry and forces in the pillar–particle–pillar system. The capillary force between pillars and particles $F_{pillar\text{-}particle}$ is larger than that between pillars and pillars $F_{pillar\text{-}pillar}$. (*B*) SEM image showing that the strong capillary force between pillars and particles may induce the configuration change of the assembled cells. (Scale bar, 2 μm.)

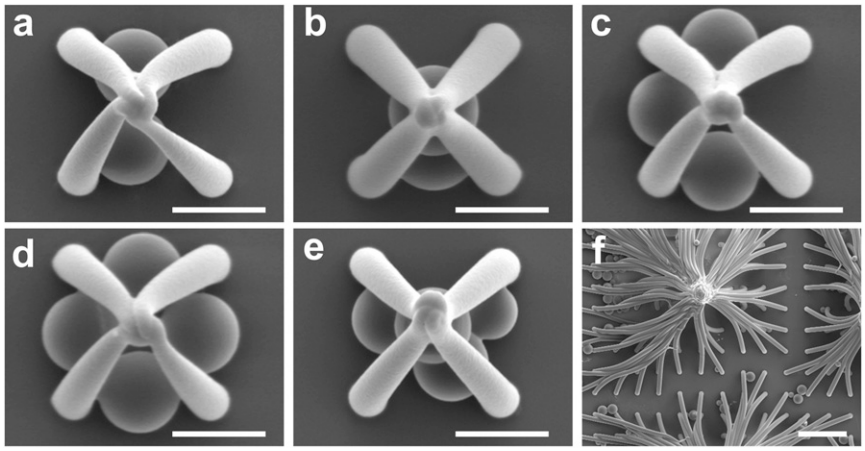

Fig. S6. (*A*–*E*) Large assembled cells may trap multiple particles at the same time. (Scale bars, 2 μm.) (*F*) Particles with different sizes can be trapped by the filamentous aggregates. (Scale bar, 10 μm.)

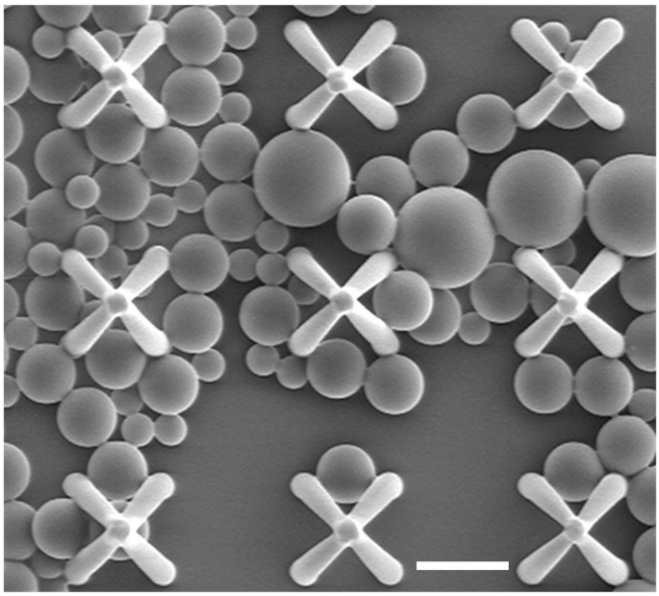

Fig. S7. High particle concentration results in aggregation. When the particle concentration is higher than 10^{-3} g/mL, the particles aggregate and trapping fails. Therefore, a concentration of 10^{-4} g/mL is used in the text. (Scale bar, 3 μm.)

Table S1. Summary of the yield percentage of assembled cells with different spacing variations and heights

Δd, μm height, μm	0.5, %	1.0, %	1.5, %	2.0, %	2.5, %	3.0, %
1	0	0	0	0	0	0
2	45	42	41	41	43	42
3	60	80.5	92	100	100	100
4	67	96	99	100	100	100
5	9.5	15.5	31	55	85	100
6	0	4.5	6.5	7	12.5	79
7	0	0	0	0	2.5	4

All of the data are obtained by optical microscope in situ observation.

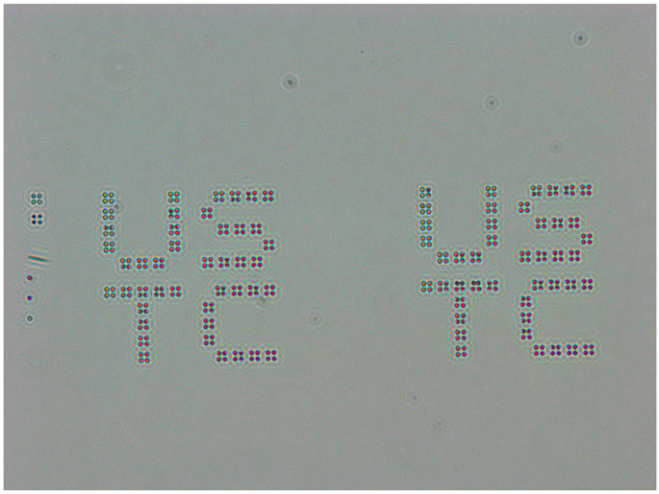

Movie S1. The reversible opening and closing of the assemblies. When the liquid evaporates, the pillars bend to form the assemblies. When the sample is immersed in liquid, the pillars return to their standing state and the assemblies open. The motion can be repeated for many cycles.

Movie S1